Desalination and Water Treatment
www.deswater.com
doi: 10.5004/dwt.2021.26988

218 (2021) 423–435
April

Dual action of both green and chemically synthesized zinc oxide nanoparticles: antibacterial activity and removal of Congo red dye

Mohamed A. Hassaan[a,*], Shimaa Hosny[b], Marwa R. ElKatory[c], Rehab M. Ali[d], Tauseef Ahmad Rangreez[e], Ahmed El Nemr[a]

[a]*Marine Pollution Lab, Marine Environment Division, National Institute of Oceanography and Fisheries (NIOF), Alexandria, Egypt, emails: Mhss95@mail.com/ma.hassaan@niof.sci.eg (M.A. Hassaan), ahmedmoustafaelnemr@yahoo.com (A. El Nemr)*
[b]*Taxonomy and Biodiversity of Aquatic Biota Lab, Marine Environment Division, National Institute of Oceanography and Fisheries (NIOF), Alexandria, Egypt, email: shimaasea@yahoo.com*
[c]*Advanced Technology and New Materials and Research Institute, City of Scientific Research and Technological Applications (SRTA-City), Alexandria 21934, Egypt, email: marwa_elkatory@yahoo.com*
[d]*Fabrication Technology Department, Advanced Technology and New Materials and Research Institute, Scientific Research and Technological Applications (SRTA-City), Alexandria, Egypt, email: rehabmohamedali1983@gmail.com*
[e]*Department of Applied Chemistry, Aligarh Muslim University, Aligarh 202002, India, email: tauseefjh@gmail.com*

Received 14 July 2020; Accepted 20 December 2020

ABSTRACT

Two routes green and chemical were used to synthesize zinc oxide nanoparticles (ZnO NPs). *Gelidium pulchellum* extract was used as a bioreducing agent in this work. The formation of ZnO NPs was evaluated by Fourier transform infrared analysis with signals at 441 and 428 cm^{-1} for green and chemically synthesized ZnO NPs, respectively. ZnO NPs exhibiting hexagonal and cubic mixed phases were observed from the transmission electron microscopy and X-ray diffraction analysis with an average particle size of 17 nm for green and 22 nm for chemical. ZnO NPs showed a considerable antibacterial activity towards gram-positive bacteria *Staphylococcus aureus*, *Bacillus subtilis*, and *Enterococcus faecalis* than toward the gram-negative one. The outcomes of this study revealed the maximum inhibition zone for gram-positive bacteria growth (*B. subtilis*) was (27.3 ± 2.5 mm) by green ZnO NPs with the concentration of 100%. While the minimum inhibition zone was (11.3 ± 0.57 mm) represented by gram-positive bacteria (*S. aureus*) by chemically synthesized ZnO NPs with the concentration of 10%. So the antibacterial influences of ZnO NPs might be related to the characteristics of definite bacterial species, the size of the nanoparticles, and the synthesis methods (physical, chemical, or biological). Decolorization of Congo red (CR) dye was 85% after the first 3 min of the contact time with ZnO NPs.

Keywords: Zinc oxide nanoparticles; Green synthesis; *Gelidium pulchellum;* Antibacterial effects; Dye removal

1. Introduction

Algae are known as "bio-nano-factories" because of their ability to synthesize metal nanoparticles [1,2]. The capacity of algae to aggregate and reduce metal particles makes them a predominant candidate for nanoparticles biosynthesis [2]. A wide-ranging of plant extract are operated for the biosynthesis of ZnO NPs including marine macroalgae [3–11].

Based on their broad biological applications, the vast field of nanotechnology and nanoparticles has extended beyond imagination. The compounds obtained from

* Corresponding author.

macroalgae are accounted for a wide scope of biological applications such as antifouling, antibacterial, and anticoagulant applications [12–14]. Antibacterial applications of nanoparticles for instance magnesium oxide, ZnO, and titanium dioxide, and their specific poisonous effect on microorganisms determine their possible usage as antibacterial agents. Some of these recent studies have shown that marine algae are ideal for using silver, gold, and zinc nanoparticles [15–22].

ZnO NPs as a semiconductor have been rising into consideration for their extensive scope of utilizations, for instance, optoelectronics, optics, biomedical, electronics, and dye removal using ecofriendly synthesis constituents like fungus, leaf extract (aloebarbadensis) bacteria, and marine macro-algae *Sargassum muticum* [3,23–28].

Gelidium pulchellum was selected in this study because it has antibacterial activities against a widespread range of gram-negative and positive bacteria and fungi such as (*Micrococcus luteus*, *Bacillus subtilis*, *Staphylococcus aureus*, *Escherichia coli*, *Enterobacter aerogenes*, *Klebsiella pneumonia*, *Candida albicans*, and *Aspergillus niger*) [29,30]. The present study describes the quick synthesis and characterizations of ZnO NPs prepared either by green technique using *G. pulchellum* or chemically and their antibacterial application, besides investigating the ability of ZnO NPs for adsorption of CR dye from aqueous solution. It is worth to mention that, this work is the first to report the usage of the aqueous extract of *G. pulchellum* as a bio-reducer for ZnO NPs synthesis.

2. Materials and methods

A schematic diagram of the experimental procedures and the phycosynthesis route of ZnO NPs can be shown in Figs. 1 and 2, respectively. The Congo red dye (C.I. 22120) ($C_{32}H_{22}N_6Na_2O_6S_2$) (Mwt = 696.67) was bought from Sigma-Aldrich (Germany) and used without any modifications.

2.1. G. pulchellum collection

G. pulchellum was carefully collected and separated from rocks substrata at the vicinity of Qait bay citadel (31.213040, 29.884139), West of Alexandria, Egypt. Algae were cleaned with tap water to eliminate impurities and the sample was examined by compound microscope following the standard taxonomic keys as described by Feldmann [31] and was confirmed using algae base website. The washed samples were dried at 60°C to achieve final moisture content <10% before being grounded into a fine powder using a blender.

2.2. Synthesis and characterization of ZnO NPs

Dried *G. pulchellum* powder (2 g) was added to 100 mL double distilled water followed by heating up to 100°C, afterwards it was filtered via filter paper 41. Before completing the reaction, the small portion of the extract was introduced to gas chromatography-mass spectrometry analysis which was carried out by following the method mentioned by Azizi et al. [3]. The gas chromatography-mass spectrometry (Agilent 7890A, USA) connected with mass detector (Agilent 5975C, USA) was used for chemical analysis of algae.

The synthesis of green and chemical ZnO NPs was carried out following the procedure mentioned elsewhere [27]. 50 mL of *G. pulchellum* aqueous extract was added to (2 mM) solution of $Zn(Ac)_2{\cdot}2H_2O$ followed by the addition of 2 M NaOH drop wise until the pH became 12. The mixture was left for 2–3 h under continuous stirring at 65°C. The pale white solid product was collected through centrifugation at 5,000 rpm for 10 min and carefully washing with DDW and left to dry at 80°C overnight. The pure ZnO NPs were gained by calcination of ZnO at 500°C for 4 h. For chemical synthesis, same procedures were followed without adding the aqueous extract of *G. pulchellum*.

The properties of green and chemically synthesized ZnO NPs using *G. pulchellum* extract were investigated by Fourier transform infrared spectroscopy (FTIR; IR Affinity-1S FTIR spectrometer Shimadzu, Japan). Raman spectroscopy were obtained using a Bruker Senterra Raman microscopy (Germany). X-ray diffractograms for ZnO NPs were obtained using a (BrukerMeasSrv (D2-208219)/D2-2082019 diffractometer) operates at 30 kV, 10 mA with Cu tube (λ = 1.54 Å) with range from 0° to 100°. The microstructure and the average size of ZnO were investigated by scanning electron microscopy (SEM; Joel 6360LA, USA) and transmission electron microscopy (TEM; Tecnai™ G2 Spirit, FEI, USA). The particle size analyzer (PSA) and the specific surface area [Brunauer–Emmett–Teller (BET)] were also measured. UV-vis spectra are observed in the 200–800 nm range.

2.3. Antibacterial effect

The indicator bacteria operated in the present examination were; *B. subtilis* ATCC 23857, *E. faecalis* ATCC 29212, *S. aureus* ATCC 6538, and *E. coli* ATCC 25922. These

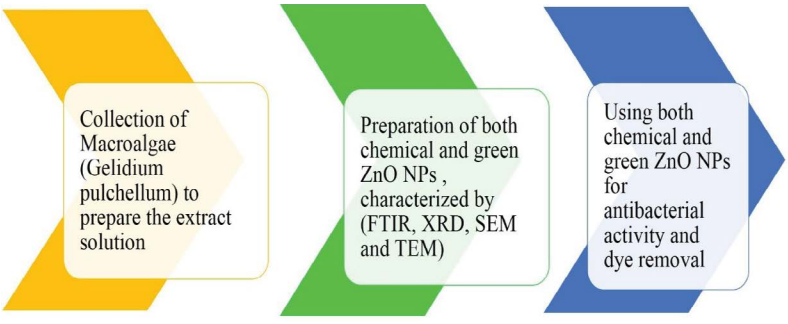

Fig. 1. Scheme of experimental procedure.

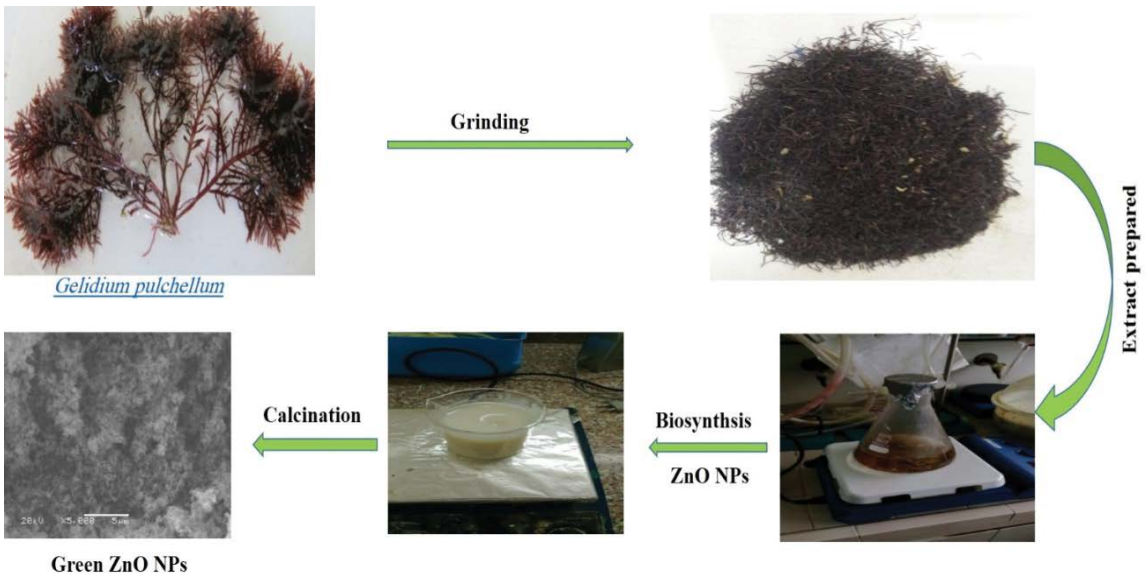

Fig. 2. Scheme of phycosynthesis route of ZnO NPs from *G. pulchellum* extracts.

were provided by the Microbiology Laboratory, NIOF, Alexandria, Egypt.

Each extract was examined to check if it contained antibacterial agents by well-cut diffusion method. 100 µL from different concentration (100%, 75%, 50%, 25%, and 10%) prepared by dilution of ZnO NPs suspension solution (1 g/100 mL) were pipetted into each well. All plates were incubated for 24 h at 37°C. After the incubation period, the radius of clear zone around each well was linearly measured in millimeter (mm). Each set was prepared in triplicate and results were expressed as mean value ± standard error of the mean of growth inhibition zones diameters obtained [32].

2.4. Congo red adsorption study

CR dye adsorption study was carried out in batch form to examine the effect of different parameters for example reaction time, adsorbent amount, and primary concentrations of dye. Dyes solutions with known concentrations were prepared and required amount of ZnO NPs was added followed by shaking on an orbital shaker, finally, the initial and residual concentration of CR dye was determined at 495 nm [17,26,28,33,34].

3. Results and discussion

3.1. Gas chromatography-mass spectrometry study

A broad range of compounds such as phenols, alcohol, esters, and ethers could be observed in the chromatogram. The gas chromatography-mass spectrometry analysis of ethanol extract of *G. pulchellum* showed 16 chemical compounds, Fig. 3. Among these compounds: 7.92 min 1-hexadecanol, 9.38 min phenol, 2,4-bis(1,1-dimethylethyl), 10.26 min 1-monolinoleoylglycerol trimethylsilyl ether, 19.38 min phthalic acid, di(2-propylpentyl) ester, and 22.12 min cholesta-3,5-diene.

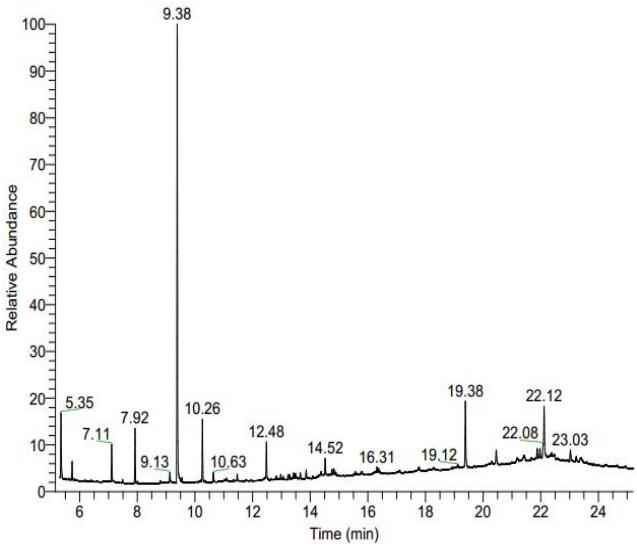

Fig. 3. GC-MS chromatogram of *G. pulchellum* extract.

3.2. FTIR analysis

The FTIR spectra were obtained by (IR Affinity-1S FTIR spectrometer Shimadzu, Japan). The signal at 441 cm^{-1} and strong E2 mode of vibration at 428 cm^{-1} verify the existence of green and chemically prepared ZnO NPs, respectively. The spectrum in Fig. 4 agrees with the previous studies (sharp significant band at 539 cm^{-1} might be corresponding to either a local vibration mode related to oxygen vacancies and zinc interstitials or to the donor defects [35]. The bands at 1,540 and 1,570 cm^{-1} correspond to the asymmetric and symmetric stretching vibrations of carboxylic group, while the broad and small peaks at 2,291 and 3,448 cm^{-1} are attributed to carbon dioxide stretching mode and hydroxyl group [36–42].

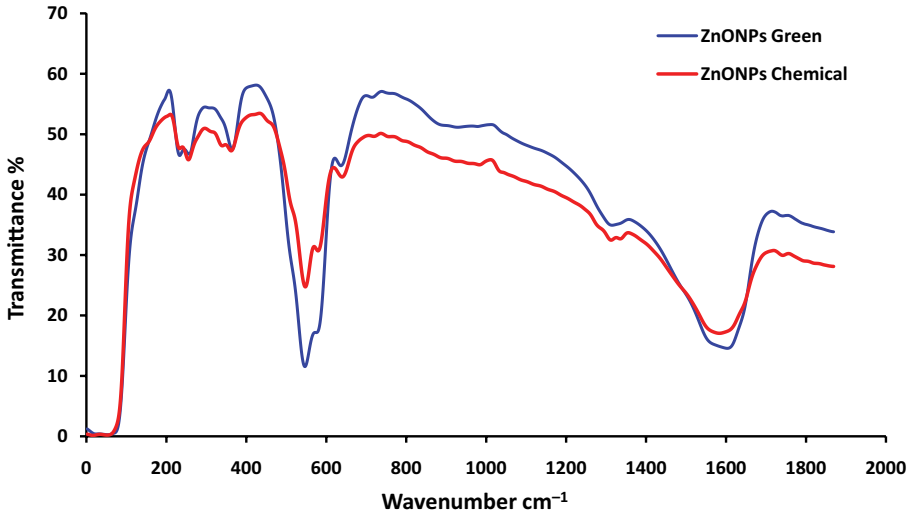

Fig. 4. FTIR spectra of green and chemical ZnO NPs.

3.3. Raman spectra analysis

The Raman spectra were obtained using a Bruker Senterra Raman microscope (Germany). The samples were excited by a laser beam of 532 nm (green laser); the samples were exposed to a laser beam for 1 s at 10 mW power with aperture 25 mm × 1,000 mm. In our investigation ZnO NPs (Fig. 5) shows prominent vibration peaks at 334, 442, and 582 cm^{-1}. A maximum peak at 442 cm^{-1} corresponds to E2. The peak at 582 cm^{-1}, situated between A1 and E1 optical phonon mode, rises due to oxygen imperfection. The peak at 334 cm^{-1} is allocated to A1 transverse mode and rises as a result of the anisotropic nature in the force constant.

3.4. X-ray diffraction pattern study

X-ray diffraction (XRD) pattern of ZnO NPs were obtained using a (Bruker Means Srv (D2-208219)/ D2-2082019 diffractometer); operates at 30 kV, 10 mA with Cu tube (λ = 1.54 Å) with a range from 0 to 100°A. Fig. 6 shows the XRD patterns of both green and chemically synthesized ZnO NPs. The peaks indicate that the ZnO powder is highly crystalline, and altogether peaks are in suitable arrangement with the cubic shape of: ZnO, 65-2880 reference pattern for both green and chemically synthesized ZnO NPs, and with a hexagonal structure of: ZnO NPs, 05-20664 reference pattern for green ZnO NPs and 65-2880 reference pattern for chemically ZnO NPs. From the above results, a mixed phase of hexagonal and cubic is present by comparing with the mentioned reference patterns. The percentage of hexagonal to cubic in green ZnO NPs is 3:1 (74.4:25.5) while the percentage of hexagonal to cubic in chemical ZnO NPs is 2:1 (66.6:33.3). The strong narrow diffraction peaks specify the well crystalline nature of ZnO NPs.

3.5. SEM study

The morphology of the nanostructure ZnO was investigated by using a SEM (Joel 6360LA, USA). Fig. 7 demonstrates the SEM analysis that confirmed the synthesized ZnO NPs. For green ZnO NPs the external surface is rod-like particles that are interconnected creating holes and thus yielding a large surface area. While the chemically synthesized ZnO NPs has a surface with nanostructures in the shape of nano-flakes and small apertures.

3.6. TEM study

The size of ZnO NPs was determined by TEM; Tecnai™ G2 Spirit, FEI, USA), operated at high voltage range of 20–120 kV/ LaB6. The TEM analysis (Fig. 8), indicates that the particles size fluctuated between 8 and 26 nm with average particle size of 17 nm for green ZnO NPs and between 11 and 39 nm with mean particle size of 22 nm for chemical ZnO NPs.

3.7. Particle size analyzer

The particle size (by PSA) and surface area of the particles were also determined. It was observed that the green ZnO NPs have uniform particle size in range of 3 nm but the chemical ZnO NPs have non-uniform particle size in the range from 3 to 4 nm as detected by 10.9° test angle Fig. 9a. While the green ZnO NPs were similar and uniform as distinguished by the 90° test angle with the range of 95 nm as shown in Fig. 9b.

3.8. Ultraviolet-visible spectroscopy analysis

UV-visible spectroscopy was carried out to study further the optical property and to determine the bandgap of the nanorods. The ambient temperature ultraviolet-visible spectra of the ZnO NPs dispersed in ethanol are presented in Fig. 10. ZnO NPs shows a strong band at 376 nm due to an excitonic transition at ambient temperature [43].

3.9. BET analysis

ZnO NPs surface area was between 27.41 and 24.84 m^2/g with varied pores – 0.07132 and 0.06205 cm^3/g for green and chemical ZnO NPs respectively, at temperature of

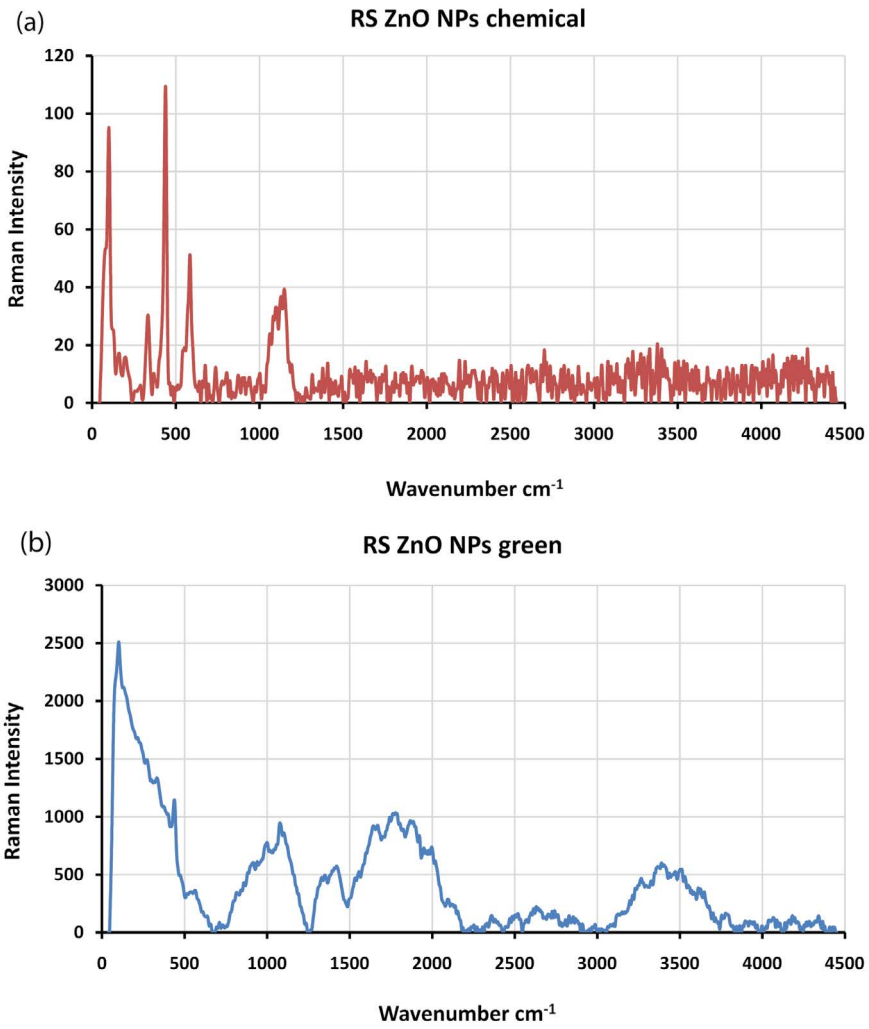

Fig. 5. Raman spectra of (a) chemical and (b) green ZnO NPs.

500°C (Table 1). The reduction in surface and pore volume as a result of different synthetic conditions such as higher calcinations temperature may minimize the pores which will lead to a reduction in specific pore volumes and surface area [44,45].

4. Antibacterial application

When ZnO NPs were tested in *B. subtilis*, *S. aureus*, *E. coli*, and *E. faecalis*, the bacterial growth was inhibited effectively (Table 2 and Fig. 11). The antibacterial effect of ZnO NPs was clearly evaluated by the occurrence of an inhibition zone. The antibacterial activity was less noticeable with the gram-negative than the gram-positive bacteria; similar outcomes were verified in the study by Zhongbing et al. [46]. In this study, it was also noticed that these are highly sensitive against different concentration of ZnO NPs s, the growing resistance has also been improved by rising the concentration of ZnO NPs. The inhibition zone area matches each type of bacteria, type of method used to synthesize nanoparticle (chemical or biological methods), and the concentration and volume of ZnO NPs. The maximum inhibition zone for the growth of gram-positive bacteria (*B. subtilis*) was (27.3 ± 2.5 mm) and it was given by ZnO NPs with concentration of 100% which were synthesized from the extract of *G. pulchellum*. While the minimum inhibition zone was (11.3 ± 0.57 mm) represented by gram-positive bacteria (*S. aureus*) and it was given by ZnO NPs with concentration of 10% which were synthesized by chemical method. It is worth to mention that the minimal concentration of ZnO NPs % which were synthesized by green method gave high inhibition zone (24.1 ± 1 mm) for the growth of (*B. subtilis*).

Gram-positive bacteria have a thicker cell wall (20–80 nm), compared to thin, 7–8 nm thick peptidoglycan layer for gram-negative bacteria. The size of nanoparticles within these ranges will easily move through the peptidoglycan, and is therefore, very harmful. According to the results and based on the TEM analysis ZnO NPs (average particles diameter 17 and 22 nm), we could assume that ZnO NPs are active antibacterial agents for both gram-positive and gram-negative bacteria. ZnO NPs are thought

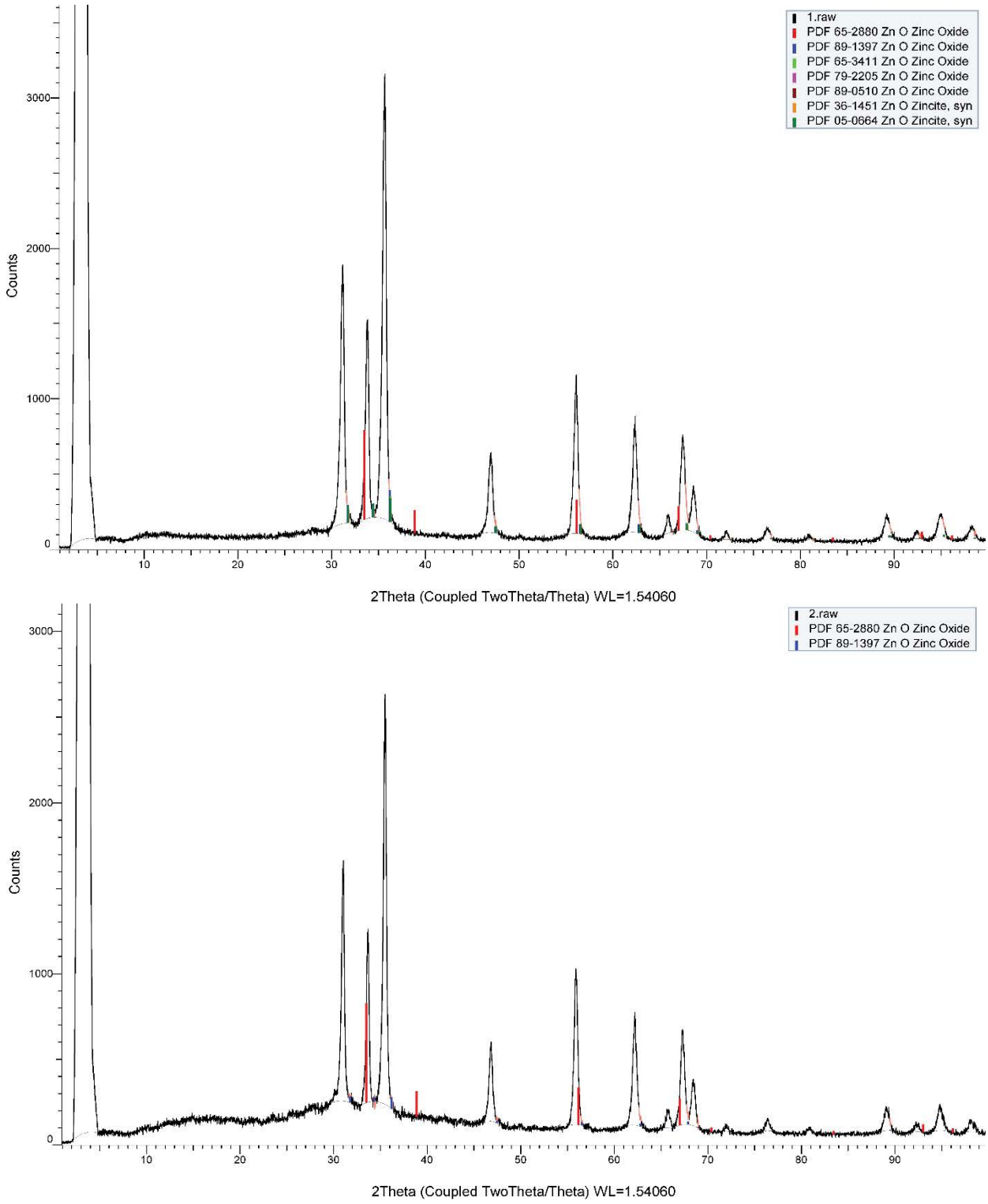

Fig. 6. XRD patterns of the synthesized green and chemical ZnO NPs.

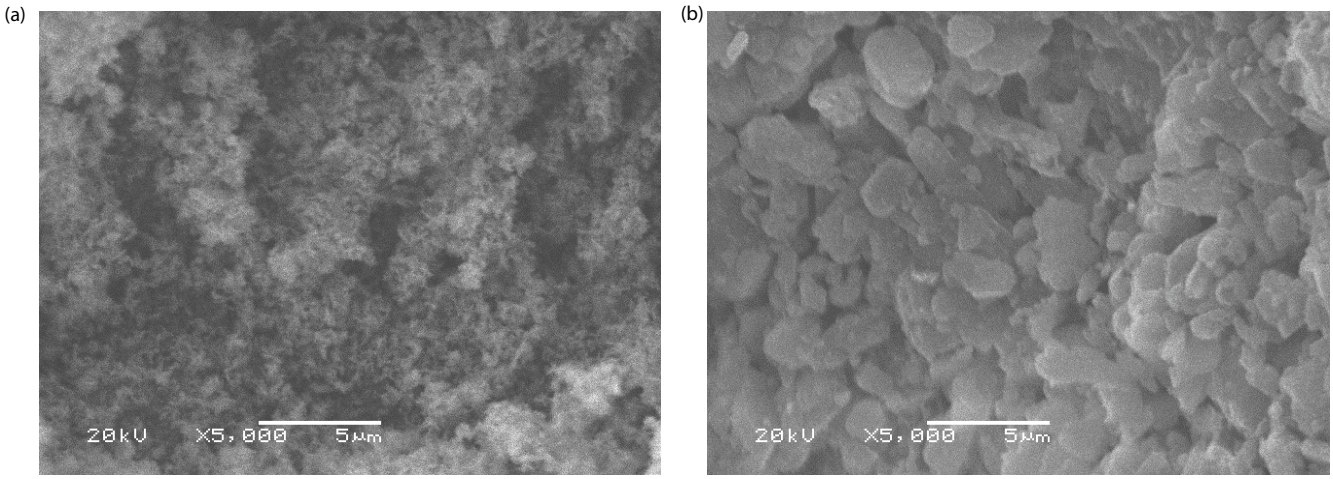

Fig. 7. SEM of (a) green and (b) chemical ZnO NPs.

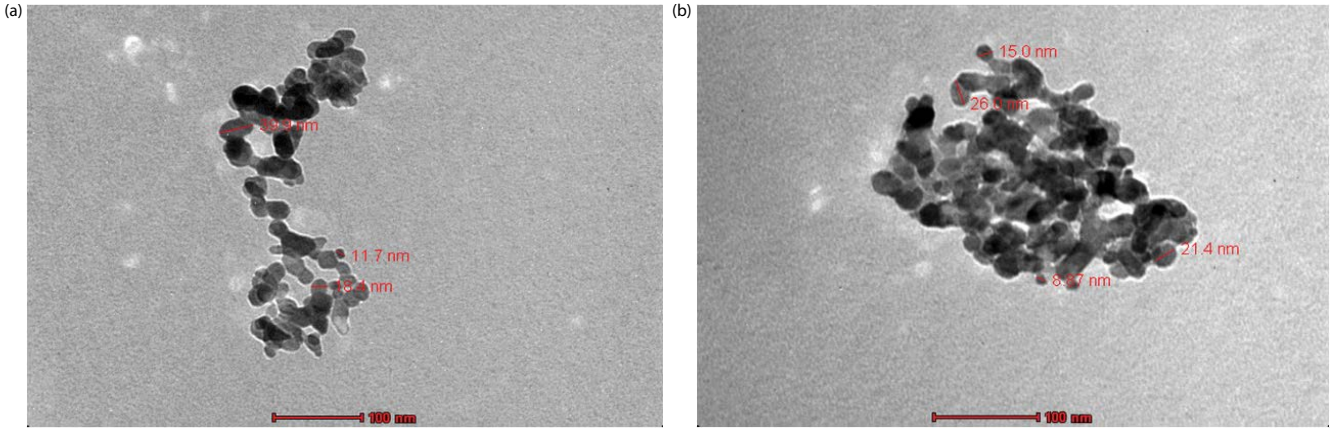

Fig. 8. TEM images of the synthesized: (a) green and (b) chemical ZnO NPs.

Table 1
BET surface area and porosity of ZnO NPs

Type	Surface area (m^2/g)	Diameter of pores (nm)	Volume of pores (cm^3/g)
Green ZnO NPs	27.41	10.40	0.07132
Chemical ZnO NPs	24.84	9.99	0.06205

to destroy bacterial cell membrane lipids and proteins, which causes the leak of intracellular components and eventually bacterial cell death [46,47]. Synthesized ZnO NPs with average particles size around 12 nm can slow the bacterial development up to 100% at 3 mM [48]. The outcome of ZnO NPs antibacterial application indicates that both green and chemically synthesized ZnO NPs are antibacterial agents, however green synthesized method was preferred because it is considered as environmentally friendly.

5. Congo red adsorption study

5.1. Influence of contact time

The impact of contact time on the elimination of the CR dye color is examined when the contact period varies from 3 to 180 min at adsorption condition of 0.1 g ZnO NPs/10 mL CR dye solution of 50 ppm with an agitation speed of 200 rpm, natural pH (pH = 6) and ambient temperature. The experiments were repeated three times. From Fig. 12 it is clear that by increasing the contact time, the

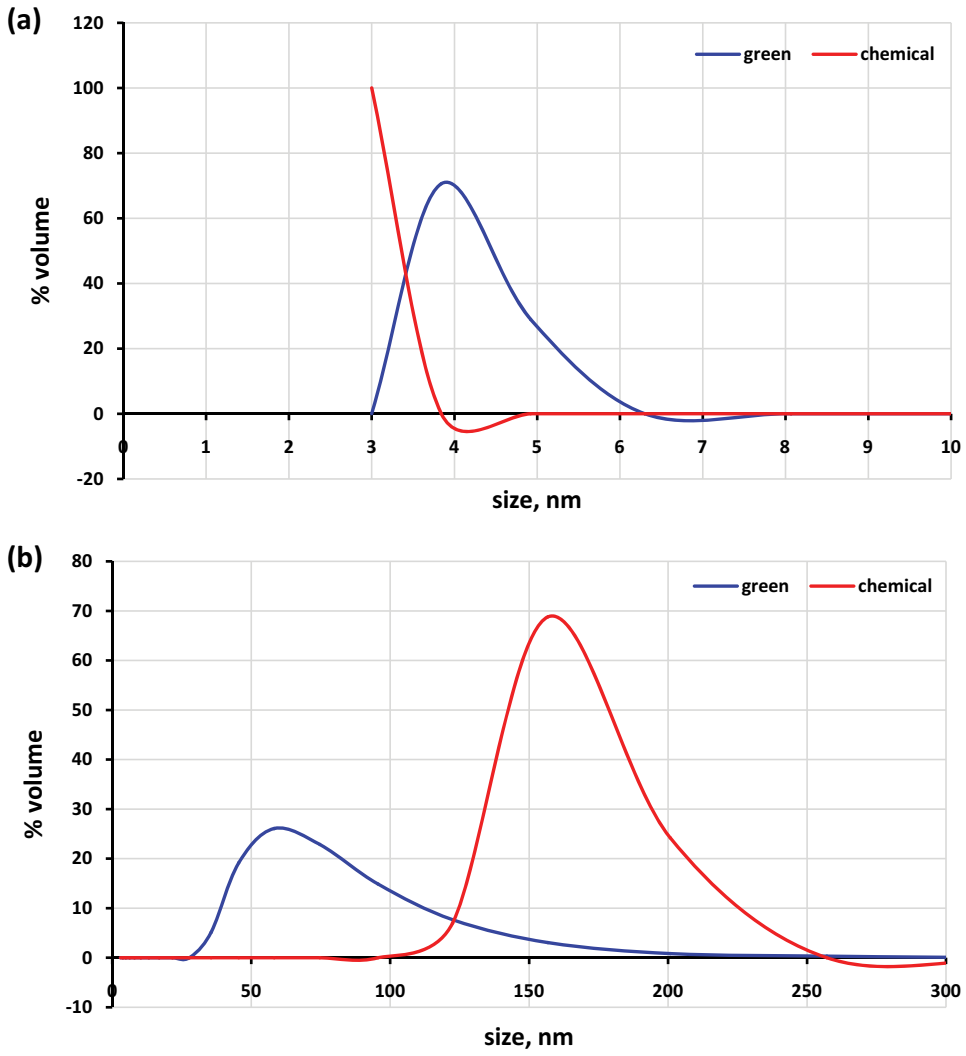

Fig. 9. PSA spectra of green and chemical ZnO NPs. PSA ZNO NPs angle: (a) 10.9° and (b) 90°.

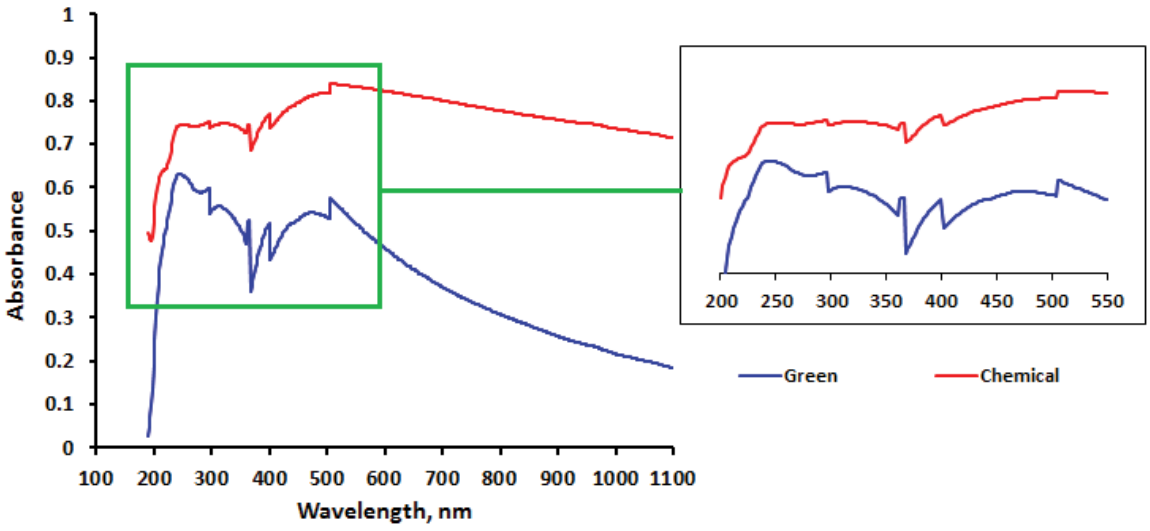

Fig. 10. UV-vis spectra of green and chemical ZnO NPs.

Table 2
Antibacterial activity from different concentration of (ZnO NPs) against gram-positive and negative bacterial pathogens

	Inhibition zone (mm) at various concentrations									
	100%		75%		50%		25%		10%	
	Chem.	Green	Chem.	Green	Chem.	Green	Chem.	Green	Chem.	Green
E. coli –	15.3 ± 0.57	15.3 ± 0.57	14.3 ± 0.57	14.3 ± 0.57	13.3 ± 1.5	14.3 ± 0.57	12.3 ± 0.57	13 ± 1	12.3 ± 0.57	12
B. subtilis +	27.6 ± 1.5	27.3 ± 2.5	22.6 ± 2.5	16.6 ± 1.5	18 ± 1	24 ± 1	18 ± 1	24.6 ± 0.57	17.3 ± 0.57	24 ± 1
S. Aureus +	16 ± 1	16 ± 1	15 ± 1	15.3 ± 0.57	12 ± 1	15.3 ± 0.57	12 ± 1	14 ± 1	11.3 ± 0.57	11.3 ± 0.57
E. Faecalis +	19.3 ± 0.57	17.3 ± 0.57	17 ± 1	17.3 ± 0.57	16 ± 1	13 ± 1	16 ± 1	15.3 ± 0.57	14.3 ± 1.5	11.3 ± 0.57

decolorization of CR dye is also improved until it reaches the highest decolorization rate of 100% and 82% after 20 min of contact time with green and chemically ZnO NPs, respectively. There is no considerable change in the CR dye removal rate after the first 20 min. The CR dye adsorption process with ZnO NPs is rapid as 85% of the CR dye was removed after the first 3 min of the contact time. This may be due to the presence of the active adsorption spots and the uncovered surface is higher in the first phase [49,50].

5.2. Influence of green ZnO NPs dose

The influence of ZnO NPs dose on the CR dye removal is examined with doses varying from 0.01 to 0.1 g/10 mL at adsorption circumstances of 20 min, 200 rpm, pH 6, and 50 mg/L dye concentration at ambient temperature. The experiments were repeated three times. The decolorization of CR dye increases slowly and attains the maximum removal of 100% using 0.1 g/10 mL (Fig. 13) due to the large available active spots and surface area which may facilitate CR dye penetration. From the experimental results, 0.1 g/10 mL of the ZnO NPs is the optimum dose for CR dye solution. Increasing the adsorbent dose above 0.1 g/10 mL may lead to accumulation/overlapping of the vacant sites of adsorption [51].

5.3. Influence of Congo red dye initial concentration

The initial concentration of CR dye ranges from 25 to 100 mg/L at the previously determined optimum operating conditions of adsorption which are ZnO NPs dose of 0.1 g/10 mL, 20 minute contact time, pH 6, and 200 rpm agitation speed at ambient temperature. The experiments are triplicated. From Fig. 14, it is clear that the green synthesized ZnO NPs leads to 100% CR dye removal for 25 and 50 mg/L dye concentrations. By increasing the initial CR dye concentration above 50 mg/L, the removal of CR dye color decreased. This may be due to the fact that at low CR dye concentrations, the percentage ratio of the amount of adsorbate ions to the vacant active sites of ZnO NPs is low resulting in more CR dye color removal Fig. 15. However, by increasing the initial CR dye concentration, the existing active sites are way fewer and henceforth the CR dye color removal is less [52–54].

6. Conclusions

The present study suggests that the capability of macro-algae to reduce metal ions makes predominant candidate for synthesis of nanoparticles. ZnO NPs synthesis was characterized by FTIR spectroscopy, Raman spectroscopy, SEM, TEM, and XRD analysis. The FTIR bands at 441 and 428 cm^{-1} for green and chemical ZnO NPs, respectively, moreover to a sharp significant band at 539 cm^{-1} representing the existence of both green and chemical ZnO NPs. According to the TEM and XRD analysis, the ZnO NPs have a mixed phase of both hexagonal and cubic structures with particle size ranging from 8 to 26 nm and 11 to 39 nm for green and chemically synthesized ZnO NPs, respectively. The results exhibited that green synthesized ZnO NPs showed greater antibacterial inhibition zone (27.3 ± 2.5 mm)

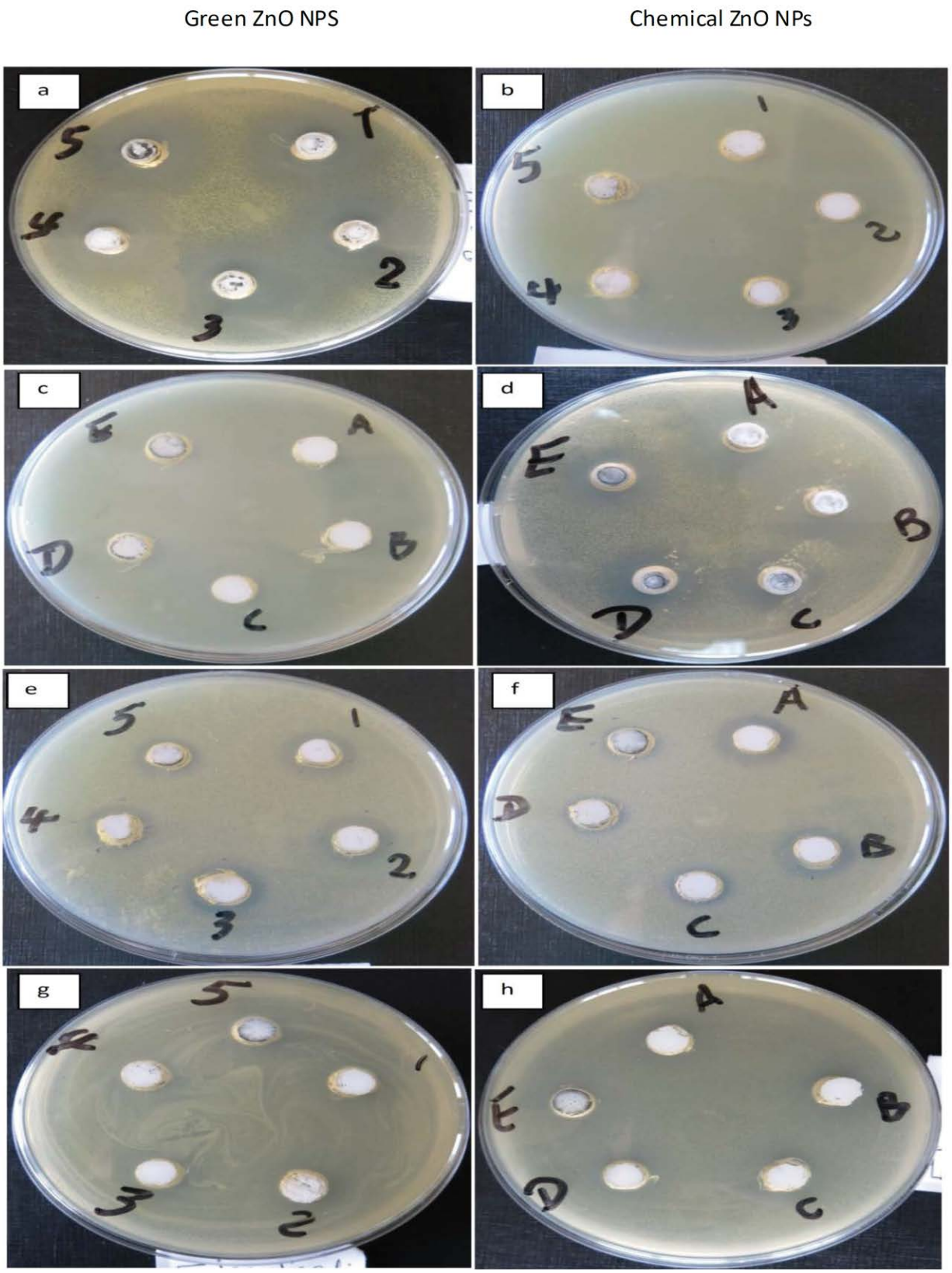

Fig. 11. Antibacterial activity with different concentration (100%, 75%, 50%, 25%, and 10% for 1-A, 2-B, 3-C, 4-D, and 5-E, respectively) of green and chemical ZnO NPs assayed by the agar well diffusion method in petri plates. ZnO NPs poured in the wells shows the zone of inhibition against (a and b) *E. coli*, (c and d) *B. subtilis,* (e and f) *S. aureus*, and (g and h) *E. faecalis*.

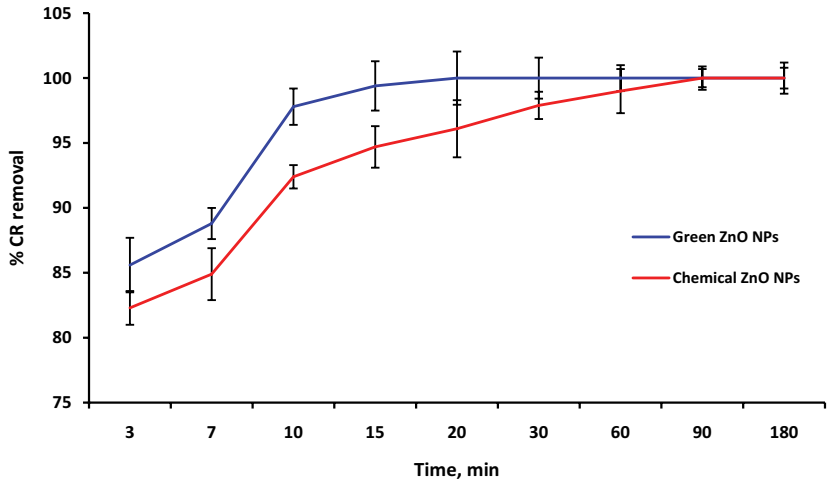

Fig. 12. Contact time effect on Congo red dye removal using green and chemical ZnO NPs.

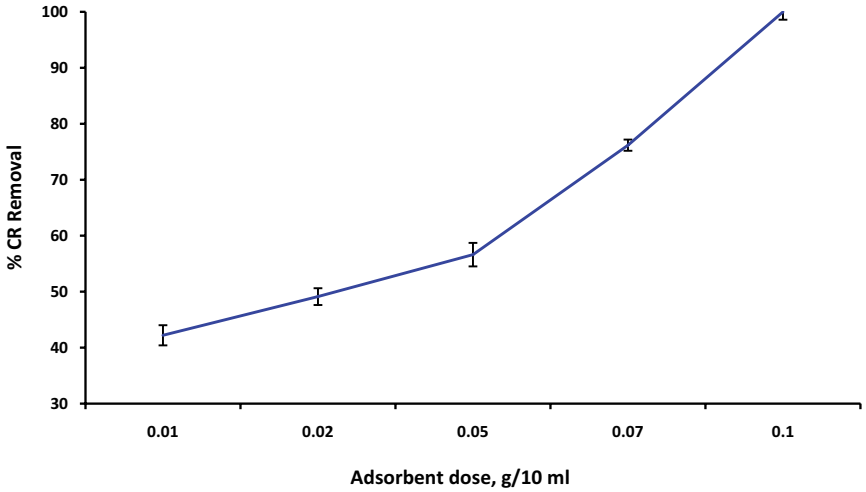

Fig. 13. Different dose effect of green ZnO NPs on Congo red dye removal.

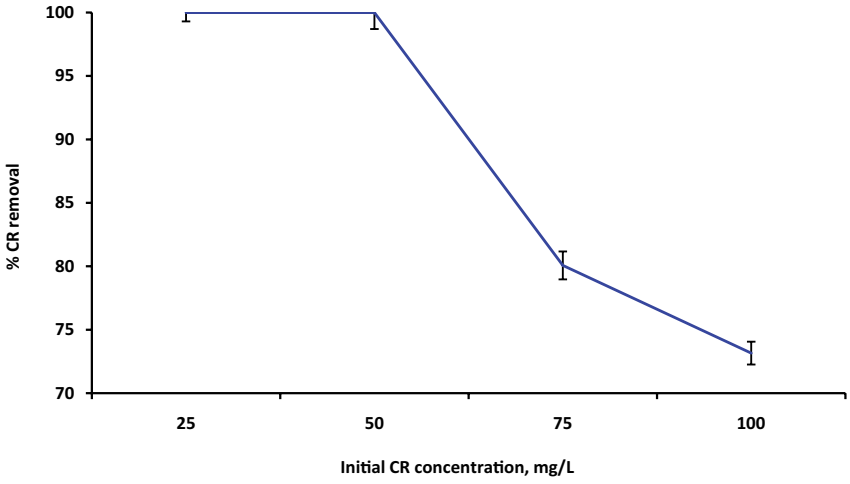

Fig. 14. Initial Congo red dye concentration effect.

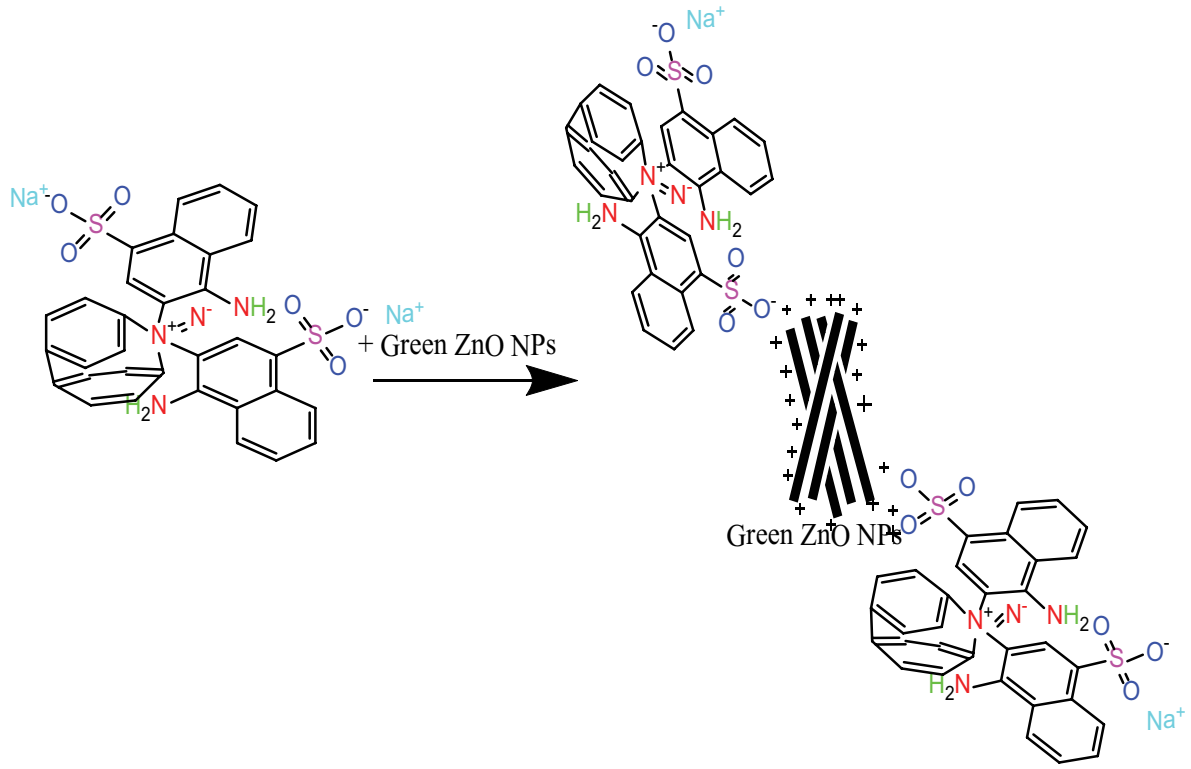

Fig. 15. Mechanism of Congo red dye removal by green ZnO NPs.

than chemical synthesized ZnO NPs (11.3 ± 0.57 mm) on both gram-positive and negative bacteria. Therefore, an environmentally friendly method using *G. pulchellum* was proposed to synthesize ZnO NPs. The green ZnO NPs were more effective than chemically synthesized ZnO NPs and showed great efficiency by completely removing the color of CR dye (100% after 20 min).

References

[1] J.Y. Song, B.S. Kim, Rapid biological synthesis of silver nanoparticles using plant leaf extracts, Bioprocess Bioassay Eng., 32 (2009) 79–84.
[2] M.A. Hassaan, A. Pantaleo, L. Tedone, M.R. Elkatory, R.M. Ali, A. El Nemr, G.D. Mastro, Enhancement of biogas production via green ZnO nanoparticles: experimental results of selected herbaceous crops, Chem. Eng. Commun., 208 (2021) 1–14.
[3] S. Azizi, M.B. Ahmad, F. Namvar, R. Mohamad, Green biosynthesis and characterization of zinc oxide nanoparticles using brown marine macroalga *Sargassum muticum* aqueous extract, Mater. Lett., 116 (2014) 275–277.
[4] N.A. Samat, R.M. Nor, Sol–gel synthesis of zinc oxide nanoparticles using *Citrus aurantifolia* extracts, Ceram. Int., 39 (2013) 545–548.
[5] P. Rajiv, S. Rajeshwari, R. Venckatesh, Bio-fabrication of zinc oxide nanoparticles using leaf extract of *Parthenium hysterophorus* L. and its size-dependent antifungal activity against plant fungal pathogens, Spectrochim. Acta, Part A, 112 (2013) 384–387.
[6] S. Gunalan, R. Sivaraj, V. Rajendran, Green synthesized ZnO nanoparticles against bacterial and fungal pathogens, Progress Nat. Sci. Mater. Int., 22 (2012) 693–700.
[7] P. Nagajyothi, T.M. An, T. Sreekanth, J.I. Lee, D.J. Lee, K. Lee, Green route biosynthesis: characterization and catalytic activity of ZnO nanoparticles, Mater. Lett., 108 (2013) 160–163.
[8] Y. Zheng, L. Fu, F. Han, A. Wang, W. Cai, J. Yu, J. Yang, F. Peng, Green biosynthesis and characterization of zinc oxide nanoparticles using *Corymbia citriodora* leaf extract and their photocatalytic activity, Green Chem. Lett. Rev., 8 (2015) 59–63.
[9] H.A. Salam, R. Sivaraj, R. Venckatesh, Green synthesis and characterization of zinc oxide nanoparticles from *Ocimum basilicum* L. var. purpurascens Benth.-Lamiaceae leaf extract, Mater. Lett., 131 (2014) 16–18.
[10] M. Darroudi, Z. Sabouri, R.K. Oskuee, A.K. Zak, H. Kargar, M.H. Hamid, Sol–gel synthesis, characterization, and neurotoxicity effect of zinc oxide nanoparticles using gum tragacanth, Ceram. Int., 39 (2013) 9195–9199.
[11] J. Qu, C. Luo, J. Hou, Synthesis of ZnO nanoparticles from Zn-hyperaccumulator (*Sedum alfredii* Hance) plants, IET Micro Nano Lett., 6 (2011) 174–176.
[12] J. Selvin, A.J. Huxley, A.P. Lipton, Immunomodulatory potential of marine secondary metabolites against bacterial diseases of shrimp, Aquaculture, 230 (2004) 241–248.
[13] S.V.P. Ramaswamy, S. Narendhran, R. Sivaraj, Potentiating effect of ecofriendly synthesis of copper oxide nanoparticles using brown alga: antimicrobial and anticancer activities, Bull. Mater. Sci., 39 (2016) 361–364.
[14] J. Selvin, A.P. Lipton, Development of a rapid 'mollusc foot adherence bioassay' for detecting potent antifouling bioactive compounds, Curr. Sci., 83 (2002) 735–737.
[15] M. Jahanshahi, Z. Babaei, Protein nanoparticle: a unique system as drug delivery vehicles, Afr. J. Biotechnol., 7 (2008) 4926–4934.
[16] K. Sobha, K. Surendranath, V. Meena, K.T. Jwala, N. Swetha, K.S.M. Latha, Emerging trends in nanobiotechnology, J. Biotechnol. Mol. Biol. Rev., 5 (2010) 001–012.
[17] M. Hassaan, M. El Katory, R.M. Ali, A. El Nemr, Photocatalytic degradation of reactive black 5 using photo-Fenton and ZnO nanoparticles under UV irradiation, Egypt. J. Chem., 63 (2020) 17–18.
[18] M. Ates, J. Daniels, Z. Arslan, I.O. Farah, H.F. Rivera, Comparative evaluation of impact of Zn and ZnO nanoparticles on brine shrimp (*Artemiasalina*) larvae: effects of particle size

and solubility on toxicity, Environ. Sci. Processes Impacts, 15 (2013) 225–233.
[19] A. Matei, I. Cernica, O. Cadar, C. Roman, V. Schiopu, Synthesis and characterization of ZnO–polymer nanocomposites, Int. J. Mater. Form., 1 (2008) 767–770.
[20] G. Kalyani, V.G. Anil, C. Bo-Jung, L. Yong-Chien, Preparation and characterization of ZnO nanoparticles coated paper and its antibacterial activity study, J. Green Chem., 8 (2006) 1034–1041.
[21] R. Amirante, G. Demastro, E. Distaso, M.A. Hassaan, A. Mormando, A.M. Pantaleo, P. Tamburrano, L. Tedone, M.L. Clodoveo, Effects of ultrasound and green synthesis ZnO nanoparticles on biogas production from olive pomace, Energy Procedia, 148 (2018) 940–947.
[22] J. Sawai, J. Yoshikawa, Quantitative evaluation of antibacterial activities of metallic oxide powders ZnO, MgO andCaO by conductimetric assay, J. Microbiol. Methods, 54 (2003) 177–182.
[23] P. Amornpitoksuk, S. Suwanboon, S. Sangkanu, A. Sukhoom, J. Wudtipan, K. Srijan, Synthesis, photocatalytic and antibacterial activities of ZnO particles modified by diblock copolymer, Powder Technol., 212 (2011) 432–438.
[24] G. Sangeetha, S. Rajeshwari, R. Venckatesh, Green synthesis of zinc oxide nanoparticles by aloe barbadensis miller leaf extract: structure and optical properties, Mater. Res. Bull., 46 (2011) 2560–2566.
[25] C. Jayaseelan, A.A. Rahuman, A.V. Kirthi, S. Marimuthu, K.T. Santhosh, A. Bagavan, Novel microbial route to synthesize ZnO nanoparticles using Aeromonashydrophila and their activity against pathogenic bacteria and fungi, Spectrochim. Acta, Part A, 90 (2012) 78–84.
[26] M.A. Hassaan, A. El Nemr, F.F. Madkour, A.M. Idris, T.O. Said, T. Sahlabji, M.M. Alghamdi, A.A. El-Zahhar, Advanced oxidation of acid yellow 11 dye; detoxification and degradation mechanism, Toxin Rev., 39 (2020) 1–9.
[27] M.A. Hassaan, A. Pantaleo, F. Santoro, M.R. Elkatory, G.D. Mastro, A. El Sikaily, S. Ragab, A. El Nemr, Techno-economic analysis of ZnO nanoparticles pretreatments for biogas production from barley straw, Energies, 13 (2020) 5001, doi: 10.3390/en13195001.
[28] M.A. Hassaan, A. El Nemr, A.A. El-Zahhar, A.M. Idris, M.M. Alghamdi, T. Sahlabji, T.O. Said, Degradation mechanism of Direct Red 23 dye by advanced oxidation processes: a comparative study, Toxin Rev., (2020) 1–10 (in Press).
[29] M. Kausalya, R.G.M. Narasimha, Antimicrobial activity of marine algae, J. Algal Biomass Utln, 6 (2015) 78–87.
[30] L.E. Hancock, M.S. Gilmore, The capsular polysaccharide of *Enterococcus faecalis* and its relationship to other polysaccharides in the cell wall, Proc. Natl. Acad. Sci. U.S.A., 99 (2002) 1574–1579.
[31] J. Feldmann, Recherches sur la Vegetation Marine de la Méditerranée: la Côte des Albères, Première Thèse, Wolf, 1937.
[32] C. Valgas, S.M. de Souza, E.F.A. Smânia, J.R.A. Smânia, Screening methods to determine antibacterial activity of natural products, Braz. J. Microbiol., 38 (2007) 369–380.
[33] R.D.C. Soltani, M. Safari, Periodate-assisted pulsed sonocatalysis of real textile wastewater in the presence of MgO nanoparticles: response surface methodological optimization, Ultrason. Sonochem., 32 (2016) 181–190.
[34] D.C.R. Soltani, A.R. Khataee, M. Mashayekhi, Photocatalytic degradation of a textile dye in aqueous phase over ZnO nanoparticles embedded in biosilica nanobiostructure, Desal. Water Treat., 57 (2016) 13494–13504.
[35] G. Nagaraju, S.A. Prashanth, M. Shastri, K.V. Yathish, C. Anupama, D. Rangappa, Electrochemical heavy metal detection, photocatalytic, photoluminescence, biodiesel production and antibacterial activities of Ag–ZnO nanomaterial, Mater. Res. Bull., 94 (2017) 54–63.
[36] O.M. Ntwaeaborwa, S.J. Mofokeng, V. Kumar, R.E. Kroon, Structural, optical and photoluminescence properties of Eu^{3+} doped ZnO nanoparticles, Spectrochim. Acta, Part A, 182 (2017) 42–49.
[37] K.D. Saravanak, S. Sivaranjani, S. Karthi, S. Pandiarajan, Synthesis and antibacterial investigation of ZnO/CNPs nanocomposite powder by hot nickel plate assisted cost effective spray pyrolysis method and its characterizations, IOSR J. Appl. Phys., 8 (2016) 16–22.
[38] D. Geetha, T. Thilagavathi, Hydrothermal synthesis of nano ZnO structures from CTAB, Dig. J. Nanomater. Biostruct., 5 (2010) 297–301.
[39] S. Suwanboon, Structural and optical properties of nanocrystalline ZnO powder from sol–gel method, Sci. Asia, 34 (2008) 31–34.
[40] S. Udayakumar, V. Renuka, K. Kavitha, Structural, optical and thermal studies of cobalt doped hexagonal ZnO by simple chemical precipitation method, J. Chem. Pharm. Res., 4 (2012) 1271–1280.
[41] R.M. Ali, M.R. Elkatory, H.A. Hamad, Highly active and stable magnetically recyclable $CuFe_2O_4$ as a heterogenous catalyst for efficient conversion of waste frying oil to biodiesel, Fuel, 268 (2020) 117297, doi: 10.1016/j.fuel.2020.117297.
[42] E.A. Soliman, M.R. Elkatory, A.I. Hashem, H.S. Ibrahim, Synthesis and performance of maleic anhydride copolymers with alkyl linoleate or tetra-esters as pour point depressants for waxy crude oil, Fuel, 211 (2018) 535–547.
[43] S. Senapati, A. Syed, S. Moeez, A. Kumar, A. Ahmad, Intracellular synthesis of gold nanoparticles using alga *tetraselmiskochinensis*, Mater. Lett., 79 (2012) 116–118.
[44] R. Sivakami, S. Dhanuskodi, R. Karvembu, Estimation of lattice strain in nanocrystalline RuO_2 by Williamson–Hall and size–strain plot methods, Spectrochim. Acta, Part A, 152 (2016) 43–50.
[45] M.A. Ismail, K.K. Taha, A. Modwi, L. Khezami, ZnO nanoparticles: surface and X-ray profile analysis, J. Ovonic Res., 14 (2018) 381–393.
[46] H. Zhongbing, Z.H. Xu, Y. Danhong, Y. Guangfu, L. Xiaoming, K. Yunqing, Y. Yadong, D. Huang, H. Baoqing, Toxicological effect of ZnO nanoparticles based on bacteria, Langmuir, 24 (2008) 4140–4144.
[47] Y. Liu, L. He, A. Mustapha, H. Li, Antibacterial activities of zinc oxide nanoparticles against *Escherichia coli* O157:H7, J. Appl. Microbiol., 107 (2009) 1193–1201.
[48] R. Brayner, R. Ferarri-Iliou, N. Brivois, S. Djediat, Toxicological impact studies based on *E. coli* bacteria in ultra fine ZnO nanoparticles colloidal medium, Nano Lett., 6 (2006) 866–870.
[49] R.M. Ali, H.A. Hamad, M.M. Hussein, G.F. Malash, Potential of using green adsorbent of heavy metal removal from aqueous solutions: adsorption kinetics, isotherm, thermodynamic, mechanism and economic analysis, Ecol. Eng., 91 (2016) 317–332.
[50] R. Sujitha, R. Kunta, Novel adsorbents possessing cumulative sorption nature evoked from Al_2O_3 nanoflakes, *C. urens* seeds active carbon and calcium alginate beads for defluoridation studies, J. Taiwan Inst. Chem. Eng., 101 (2019) 50–63.
[51] J.N. Edokpayi, J.O. Odiyo, T.A.M. Msagati, E.O. Popoola, A novel approach for the removal of lead II; ion from wastewater using mucilaginous leaves of *Dicerocaryum eriocarpum* plant, Sustainability, 7 (2015) 14026–14041.
[52] M.A. Hassaan, A. El Nemr, F.F. Madkour, Testing the advanced oxidation processes on the degradation of Direct Blue 86 dye in wastewater, Egypt. J. Aquat. Res., 43 (2017) 11–19.
[53] A. El Nemr, M.A. Hassaan, F.F. Madkour, Advanced oxidation process (AOP) for detoxification of acid red 17 dye solution and degradation mechanism, Environ. Process., 5 (2018) 95–113.
[54] M.A.O. Badmus, T.O.K. Audu, B.U. Anyata, Removal of lead ion from industrial wastewater by activated carbon prepared from periwinkle shells *typanotonus fuscatus*, Turk. J. Eng. Environ. Sci., 31 (2007) 251–263.